Structure and Photoluminescence of Pure and Indium-Doped ZnTe Microstructures

ARTICLE *in* THE JOURNAL OF PHYSICAL CHEMISTRY C · JANUARY 2011

Impact Factor: 4.77 · DOI: 10.1021/jp1069237

THE JOURNAL OF PHYSICAL CHEMISTRY C

ARTICLE

pubs.acs.org/JPCC

Structure and Photoluminescence of Pure and Indium-Doped ZnTe Microstructures

Weichang Zhou,[†,‡] Dongsheng Tang,[†] Anlian Pan,[‡] Qinglin Zhang,[‡] Qiang Wan,[‡] and Bingsuo Zou[*,§,‡]

[†]Key Laboratory of Low-Dimensional Quantum Structures and Quantum Control of Ministry of Education, College of Physics and Information Science, Hunan Normal University, Changsha 410081, People's Republic of China

[‡]School of Physics and Microelectronics Science, Hunan University, Changsha 410082, People's Republic of China

[§]School of Material Science and Engineering, Beijing Institute of Technology, Beijing 100081, People's Republic of China

ABSTRACT: High-purity and doped ZnTe microstructures were synthesized with a single thermal evaporation method. The morphology of doped ZnTe microstructures shows multilayered periodical structure, which is due to the incorporation of In elements. The PL investigation demonstrated that the pure ZnTe microstructures emit only green light (close to the bandedge) while ZnTe doped with varied In concentrations emit red or infrared light without band-edge emission. These emission changes reflected that the Donor−Acceptor pair state transition can be tuned in semiconductor microstructures for future applications.

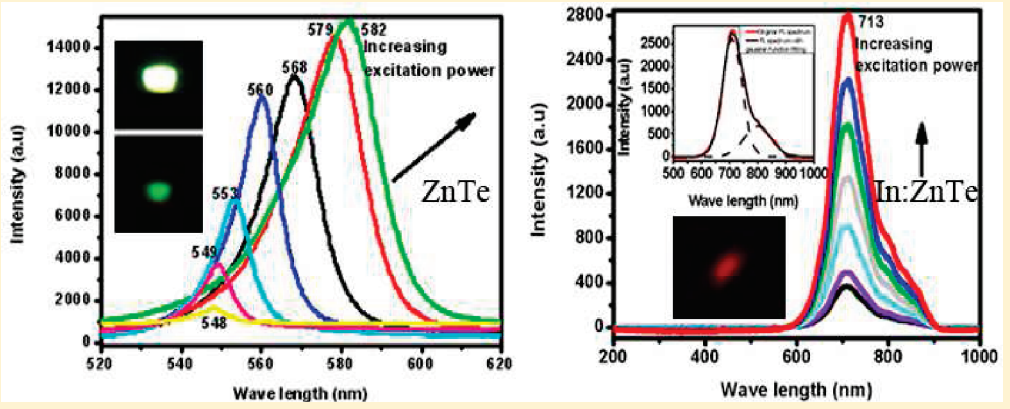

1. INTRODUCTION

One-dimensional (1-D) semiconductor nanostructures have attracted much attention due to their unique electronic, optical, and optoelectronic properties and their potential novel applications in nanodevices.[1−4] Among these nanometer-scale semiconductor materials, II−VI semiconductor nanostructures have been investigated widely and demonstrated potential application in lasers,[5] optical waveguides,[6] photodetectors,[7] and field effect transistors.[8] Zinc telluride (ZnTe), as a direct semiconductor with a band gap of 2.28 eV (~545 nm) at room temperature, is an important member of the II−VI family and an attractive material for various optoelectronic devices, such as green LEDs and photovoltaic cells.[9,10] There are many reports on the photoluminescence of ZnTe thin film or bulk material.[11,12] To date, there were only some works available on the preparation and optoelectronic properties of 1-D ZnTe nanostructures.[13−16] The low and room temperature PL spectra of single crystalline ZnTe nanowires, synthesized via the vapor phase transport method, showed near band-edge emission.[16] According to the energy band theory, the emission wavelength and hence the emitted color is based on high-purity quality and band-edge emission. The bandgaps of its binary or typically unintentionally doped semiconductor nanostructures can hardly be tuned for their definite components, which restricts their further application in different fields. This situation can be improved by doping semiconductor nanostructures, which may modulate the band gaps or produce deeptrap, thus emitting light of varied wavelengths, which sometimes simultaneously changes its phase structure.[17] For example, Peng et. al[18] showed that doped ZnSe nanocrystals with different dopant concentrations can emit tunable color light while still holding matrix ZnSe crystal phase structures. Therefore, intentional doping can greatly modify the electronic states and therein emissions of II−VI semiconductor nanostructures.

To the best of our knowledge, there are no reports so far about the synthesis of In doped ZnTe microstructures and their effect on the PL properties of ZnTe. In the present work, we focus on the incorporation of Indium into ZnTe microstructures and study their PLs. Indium is selected as the dopant because it is recognized as one of the most efficient elements used to improve the opto-electrical properties of compounds.[19] For comparison, we also synthesized pure ZnTe microstructures. The pure ZnTe microstructures show a green emission, whereas doped ZnTe microstructures show a red or infrared emission for their different dopant concentrations. Our results indicated a modulated PL emission from green to red or infrared due to the intentional doping with different dopant concentrations. Such novel red or

Received: July 25, 2010
Revised: November 24, 2010
Published: January 5, 2011

infrared light emissions are expected to have potential applications in various micro/nano-optoelectronic devices in the visible or infrared range.

2. EXPERIMENTAL METHODS

The ZnTe and In-ZnTe microstructures were synthesized by a physical evaporation method. Appropriate amounts of commercial grade ZnTe powder were placed onto a ceramic boat at the center of a quartz tube, which was placed into a horizontal tube furnace. Next to the ceramic boat, several pieces of silicon slices coated with 5 nm Au film were placed downstream of the gas flow. High-purity Ar(95%)/H_2(5%) was injected into the quartz tube with a constant flow rate (100 SCCM) to eliminate the O_2 inside before heating. The flow rate of Ar/H_2 gas was adjusted to 10 SCCM after 90 min and the furnace was rapidly heated to 1000 °C and maintained for about 60 min without changing any conditions. When the furnace cooled down, pale red products are deposited onto the surfaces of the silicon slices in the temperature range of 450−550 °C. For In doped ZnTe microstructures, we used mixed Indium powder and the above ZnTe powder as the source materials. In our present typical synthesis, the mixed powder of ZnTe and In of 10:1 and 5:1 weight ratios, respectively, are used as source materials, and their related products are marked as samples A and B, respectively. The doped ZnTe microstructures were obtained at 1000 °C for about 30 min, with black products deposited on the surface of the Si substrates.

After the synthesis, FE-SEM (JSM-6700F), XRD (using a D/max 5000 utilizing CuK_a radiation), and TEM (JEM-3010) were used to examine the morphology and phase structures of as-prepared microstructures. The Photoluminescence (PL) and Raman spectra were obtained by Scanning Near-field Optical Microscopy (SNOM, alpha 300 series, WITec GmbH, Ulm Germany) using an Ar^+ laser with a wavelength of 488 nm as the excitation source at room temperature.

3. RESULTS AND DISCUSSION

3.1. SEM of As-Prepared Pure and Doped ZnTe Microstructures. Figure 1a is the SEM morphology of high-purity ZnTe microstructures. These microstructures have smooth surfaces and lengths of up to tens micrometers. The inset shows that the diameter is about 200 nm. Figure 1b−f shows the morphology of doped ZnTe microstructure growth on Au-coated Si substrates. Figure 1b,c shows the result of using the mixture of 10(ZnTe):1(In) as the source material (sample A) while Figure 1d,e displays the results for the mixture of 5(ZnTe):1(In) (sample B). These doped microstructures have diameters ranging from 200 nm to 1 μm and lengths of tens micrometers, in general, and evidently show different geometrical shapes. The typical high-magnification SEM images (Figure 1c,e) reveal that their geometrical shapes are remarkably multilayered periodical structures. The different morphologies of pure and doped microstructures are attributed to the In incorporation into ZnTe crystal lattice, which results in significant lattice mismatch, this can be evidenced by the same morphologies for samples A and B, respectively. EDS attached on SEM can be used to describe the composition of doped products (see the inset of Figure 1c,e). There are about 1.15% and 1.86% In for samples A and B, respectively, except for Zn and Te elements. Although the In concentration is low and less than that in the source material, the low In dopant concentration changes the morphology dramatically.

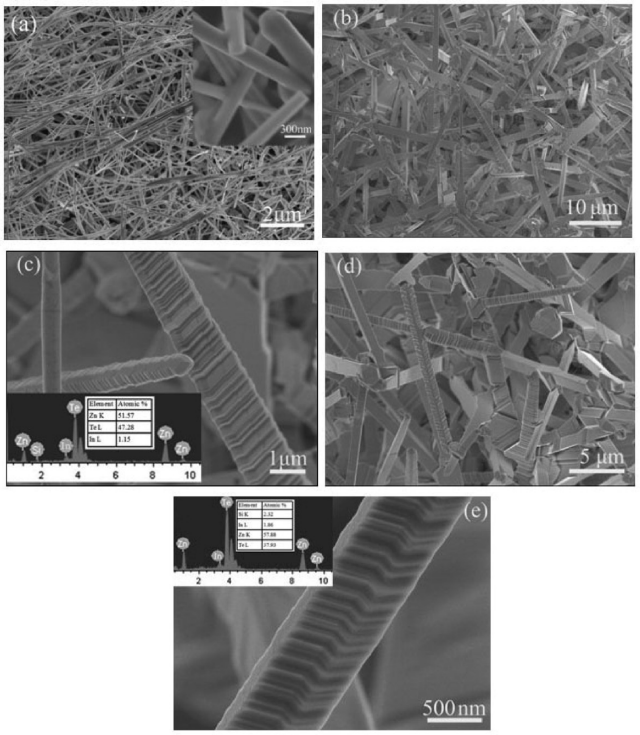

Figure 1. (a) SEM of high-purity ZnTe microstructures, inset is higher magnification SEM; (b,c) In doped ZnTe microstructures by using the mixture of 10(ZnTe):1(In) as source material, the inset in (c) is the corresponding EDS; (d,e) In doped ZnTe microstructures by using 5(ZnTe):1(In) as source material, the inset in (e) is the corresponding EDS.

Furthermore, we find that the doped microstructures are not stoichiometrically uniform, and the more In powder used in the source material, the more Zn:Te nonstoichiometric proportion is found in the final products. Therefore, many impurities sites occur in the doped microstructures and then affect the optical properties.

According to the SEM and EDS observation, we can propose a possible growth process for the doped multilayered periodical microstructures: ZnTe and In powder were vaporized under elevated temperature, then the vapors were carried by Ar/H_2 gas and transported to the downstream Si slides; then ZnTe and In vapor reacted together with Au and formed little alloy droplets. Due to the different saturation ratios of ZnTe and In, solid ZnTe precipitated from the droplets in the form of 1-D microstructures at first when it reached its supersaturated concentration. During the persistent 1-D ZnTe growth, indium dynamically precipitated and incorporated to substitute zinc sites partly along the growing 1-D ZnTe microstructures when it reached the active growth region and then may accumulate for the next precipitation step. Due to the lack of sufficient In atoms, the ZnTe growth cannot be stopped. Such In incorporation happens over time, leading to periodical structures. Such a persistent ZnTe and periodical In precipitation mechanism is similar to the alternate 1-D and 0-D growth of In_2O_3 nanotowers.[20] Without the oxidant, In atoms may incorporate into the lattice in varied valence states, possibly in In(0), In(I), In(II), and In(III). Distinct from the homogeneous In_2O_3 nanotowers, there is an internal strain in In-ZnTe due to the presence of In^{3+} with r = 0.81 Å substituting for Zn^{2+} with r = 0.74 Å . For In(0),(I),(II)

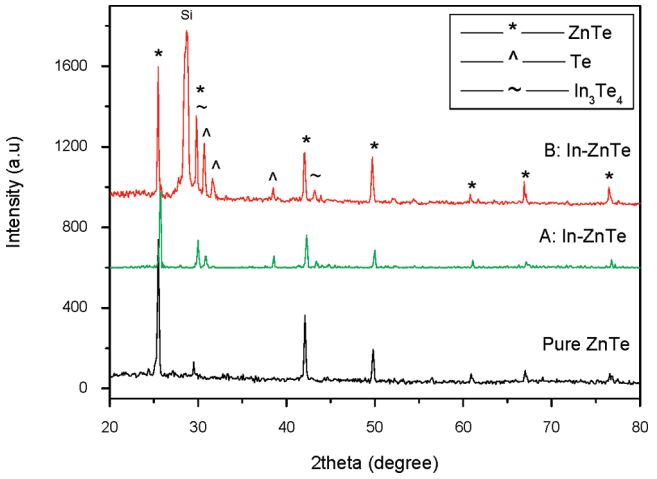

Figure 2. Normalized XRDs of pure ZnTe and doped ZnTe microstructures with different dopant concentration, respectively. The strongest diffraction peak of sample B comes from the silicon wafer substrate.

with larger radii than that of In(III), the strain should be even larger. This large difference of ionic radius between Zn^{2+} and In resulted in dramatic structural fluctuation, hence leading to a clear intermediate growth rate variation for ZnTe crystal growth, and a multilayered periodical structure under discontinuous feeding of evaporation gas due to In gas intervenes. Summarily, the alternating precipitation of indium accompanied with persistent precipitation of ZnTe is key to changing the diameter and ultimately results in the diameter-modulated feature in some regions in the present 1-D doped microstructures.

3.2. XRD of As-Prepared Pure and Doped ZnTe Microstructures. The structures of as-grown pure and doped ZnTe microstructures are determined by XRD (see Figure 2). All of the XRD diffraction peaks of pure ZnTe can be assigned to the cubic ZnTe structure with lattice constants of a = 6.1026 Å, consistent with the standard data. With the exception of the standard ZnTe diffraction peaks, there are some diffraction patterns from Te and In_3Te_4 in the doped ZnTe microstructures. This result indicates that the doping growth process is complex and In has multivalent states in the doped structure, even to In(III), some Zn may fly away during growth and Te separate out due to the thermal decomposition. Some ZnTe gas may be reduced to Te(g) by heating. Te(g) can oxidize the In atoms to different valence states for the next incorporation step. Because the oxidation power of Te(g) is not strong, some Te may be left and deposited with elemental state. When Indium doped into ZnTe crystal, In atoms or ions may substitute for some zinc to form a minor In_3Te_4 compound within ZnTe. Some elemental Te may detach from the ZnTe crystal and deposit onto the surface of the Au-coated silicon substrate. According to the EDS of a single microstructure (see the inset of Figure1c,e), we find that the content of Te is less than that of Zn, which suggests that some Te does detach from the ZnTe crystal when the Zn go out. Moreover, according to HRTEM (see Figure 3d), we can see that the single microstructure is a single-phase structure. Therefore, the detached Te deposits separately on the Si substrate and does not attach onto the doped microstructures. These diffraction peaks of impurity suggest that there may be various local defects, such as impurities, vacancies, or dislocations, in the doped microstructures. Furthermore, the diffraction intensity of impurity is weaker than that of ZnTe, which indicates a low content of In, as

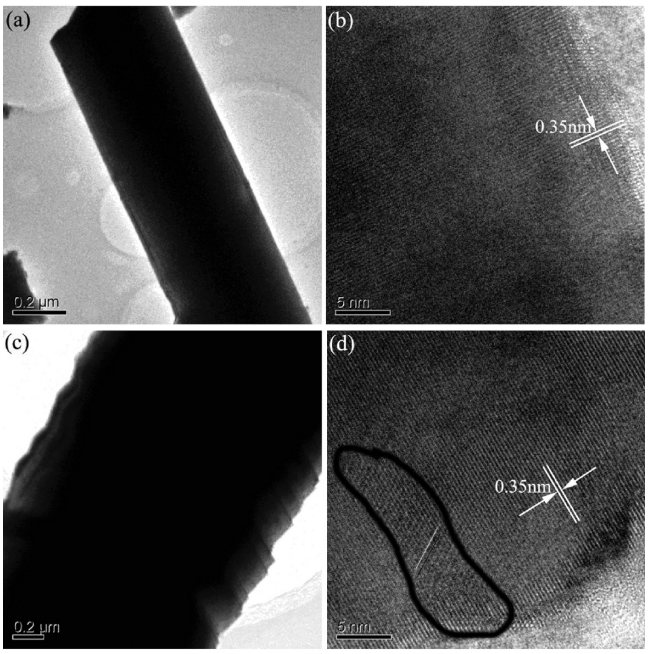

Figure 3. (a) TEM of high-purity ZnTe microstructures; (b) HRTEM of high-purity ZnTe microstructure; (c) TEM of doped ZnTe microstructures (1.15% In); and (d) HRTEM of doped ZnTe microstructure (1.15% In).

EDS indicates. The strongest diffraction peak is [111] in three XRDs and may suggest the [111] direction as the primary growth direction in these 1-D microstructures, and that the dopant does not change the growth direction of ZnTe. In fact, this argument is not determined. The [111] growth direction is well accepted to be the most densely packed surface for fcc structure in nanostructure growth. We will further discuss their growth directions according to the HRTEM observations.

3.3. TEM and HRTEM of Pure and Doped ZnTe Microstructures. The phase, growth orientation, characteristics of crystal lattice, and so forth of pure and doped ZnTe microstructures were further characterized with TEM and high resolution TEM (HRTEM). Figure 3a is the low magnification TEM of pure ZnTe microstructures with diameters of 300 nm. The surface of pure ZnTe microstructure is very smooth, which is consistent with the SEM result. But its surface contains some amorphous layers, which may influence its optical properties. The reason for this phenomenon is also related to the Te detachment. Figure 3b shows its HRTEM. The HRTEM lattice image confirms the single-crystalline structure of as-prepared microstructures. Furthermore, the measured lattice stripe spacing in HRTEM is 0.35 nm, corresponding to the interplanar distance of (111) planes as known from bulk cubic ZnTe crystal. Therefore, the growth orientation of pure ZnTe microstructures is assigned to be [111].

We also carried out the TEM and HRTEM measurements of doped ZnTe microstructures (1.15% In). Figure 3c is the typical TEM image of the doped microstructure. Different from the smooth surface of pure microstructures, the doped microstructure surface shows periodical paired zigzags along the long axis. Figure 3d corresponds to the HRTEM image. A diameter-modulated feature is clearly observed. Such HRTEM images also show single-crystalline structure. The measured lattice stripe spacing in HRTEM is also 0.35 nm, which corresponds to the

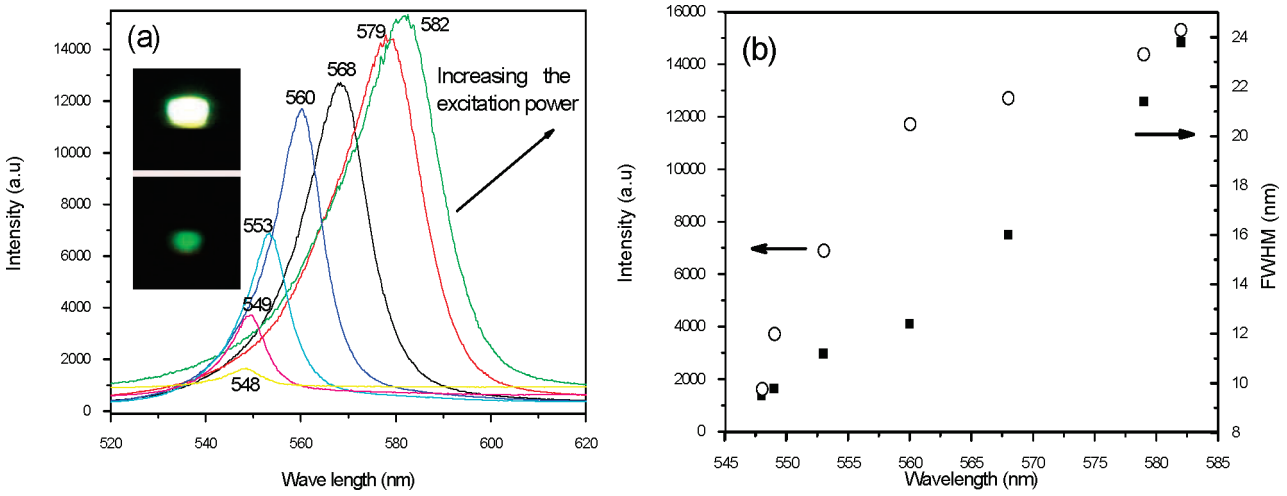

Figure 4. (a) The PL of pure ZnTe microstructures under different excitation power at room temperature; Insets are the far dark-field emission images under high and low excitation power, respectively. (b) Intensity and fwhm variation of bandgap or near- bandgap emission under different excitation power.

interplanar distance of (111) planes of doped ZnTe crystal. (The variation of lattice stripe spacing due to the low doped concentration of In is small and within the measurement error.) In this HRTEM image, we also find another orientation region(within labeled cycle zone) with an angle of 60° to the [111] stripe lines, which should be that modified by In doping. Therefore, the growth orientation of doped ZnTe microstructures can also be assigned to [111]. The minor In doping just changes the local structure periodically, which leads to a slight modification of growth direction, but does not change the growth direction in the doped microstructures. Since XRD patterns are mainly determined by their selection rules, we cannot assign this pattern profile to the orientation of [111] through examination, although some reports indicate that this argument is possible.[21,22]

3.4. PL Characterization of Pure ZnTe Microstructures at Room Temperature. As is well-known, photoluminescence (PL) is a sensitive noncontact and nondestructive technique for the measurement of the band structure and trapped states in semiconductors and can be used to characterize defect states, such as substitutional impurities (donors and acceptors) and native or intrinsic defects in semiconductors. Figure 4a is the PL characterization of high-purity ZnTe microstructures. The inset in Figure 4a is the far dark-field optical image of the ZnTe microstructure under excitation of Ar^+ laser (488 nm). We can observe by the naked eye that the green light emission of ZnTe (see the bright facula in the lower inset of Figure 4a) under low laser excitation power. The emission intensity increases and the emission band becomes broader at higher excitation power, and the emission color gradually changes from green to yellow, or even white. This variation can be verified by the corresponding PL spectra under different excitation powers. At low excitation power, the emission band is located at 548 nm, which is related to the bandedge emission of ZnTe (2.28 eV) at room temperature.[23]

The PL of semiconductor nanowire or microwire usually originates from the radiative recombination of exciton or photoinduced carriers, both local and/or delocalized. The magnitude of exciton binding energy is critical to the stability of exciton at the circumstance temperature. As the exciton binding energy 12.9 meV is lower than the kinetic energy (26 meV) at room temperature, so the free exciton cannot be present due to thermal dissociation, hence the delocalized carriers near the band-edge can be dominant with significant phonon scattering. The data from Landolt-Börnstein III/44B[24] indicate that the free exciton binding energy of ZnTe is in the range of 11−17 meV, and many shallow doping impurities have binding energies of less than 7 meV. These binding energy values in ZnTe cannot overrun the thermal dissociation force to avoid dissociation, while pure ZnO crystal can keep exciton and show exciton emission at room temperature. Therefore, the emission near the band-edge of pure ZnTe is from the radiation transition between delocalized carriers, which is broad due to the phonon and surface scattering in 1-d carrier transport.[25]

With rising excitation power, emission intensity increases for more carriers were produced, at the same time the emission bands redshift from 548 to 582 nm and become broader. It is well-known that the emission usually occurs near the band-edge in bulk direct semiconductors at room temperature, for most II−VI semiconductors have exciton binding energies less than or comparable to kT(26 meV) at room temperature, with the exception of ZnO. So the photonexcited carriers are the origin of radiative recombination. More carriers at higher excitation undergo strong coulombic repulsion forces due to the band-filling effect.[25,26] The population of newly produced carriers goes to a lower energy, which behaves in such a way that the apparent band-edge shrinks to a lower energy, therefore the optical transitions do the same. All of the shifts under varied excitation power can be assigned to exciton−carrier and exciton−phonon interactions near the dynamic band-edge. The surface amorphous layer, indicated by the HRTEM characterization (Figure 3), can enhance the exciton dissociation and the surface scattering even in CdS nanowires.[25] Hence the more carriers are produced, the more redshift due to the bandgap renormalization and plasma effect occurs.[26] This character reflects the low exciton stability and possible relaxation due to surface structural imperfections. Figure 4b shows that the emission intensity increases rapidly with excitation power and then gradually saturates under high excitation power, reflecting the typical features of electron−hole plasma in semiconductors. For the lD transport, we did not see the intensity decrease due to saturation, but rather a slow increase instead.

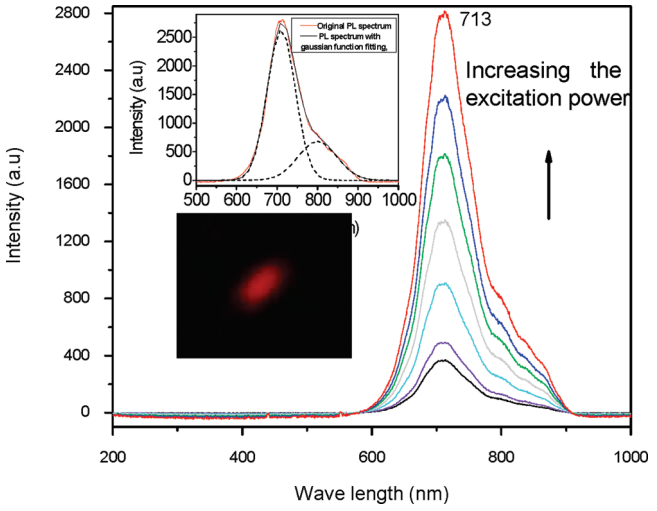

Figure 5. The PL of doped ZnTe microstructures with 1.15% In under different excitation power at room temperature; Upper inset is the fitted PL spectrum of a representative spectrum with Gaussian function; Lower inset is the far dark-field emission image under laser excitation.

3.5. PL Characterization of Doped ZnTe Microstructures with Different In Concentrations. For wide band gap semiconductors, doping often induces dramatic changes in electrical and optical properties.[26,27] We have observed their changes in morphology (see Figure 1). Figure 5 is the PL spectra of doped ZnTe microstructures with 1.15% In concentration (sample A). The left-bottom inset in Figure 5 is the dark-field image under excitation when the laser is focused on a selected area in a representative microstructure. The sample emits red light under excitation. The PL spectra show that the emission band maximum locate principally at 713 nm with a multipeak profile (this spectra can be fitted with more minibands) while the band edge emission (548 nm) cannot be detected. Furthermore, the emission peak location and line shape show no change at rising excitation powers. Since the energy of this emission peak shows no shift with excitation power, it is considered to be bound state recombination at local donor−acceptor (possibly In(0)−In(III) or In(0)−Zn vacancy). There are two reasons for its assignment. (1) Its location is far from the bandedge, which is usually due to the deeptrap emission.[23,28] In this system, the deeptrap may come from the In or Zn vacancy. The latter emission is often at 580−600 nm, so In deeptrap is more possible. (2) In usual cases, if the emission is related to the itinerant carriers, then we find that it shifts with greater carrier population. Here we find no shift, so its local transition nature is definite. Because of the multivalent (multilevels) state of the In dopant, the multilevel profile can be observed, as in Figure 5. This multilevel energy is within the bandgap of ZnTe, so the In dopant can be seen as a color center in the crystal.

Most of the excited carriers under excitation are trapped (less than 1 ps) by acceptor levels or defect centers in doped semiconductors, making the luminescence dominant through the trapped state recombination. In the present PL spectra, the origin of red emission in doped ZnTe microstructures can be attributed to excitons bound to the doped indium levels because single In(I) has an excess of electrons, which may lead to complicated emission profiles if an In(III) or a vacancy acceptor exist. Indium atoms usually acted as deep-lying donors and the formed indium donor level lies 0.4−0.6 eV beneath the conduction band in sulfide;[29,30] however, the DX state usually shifts with rising

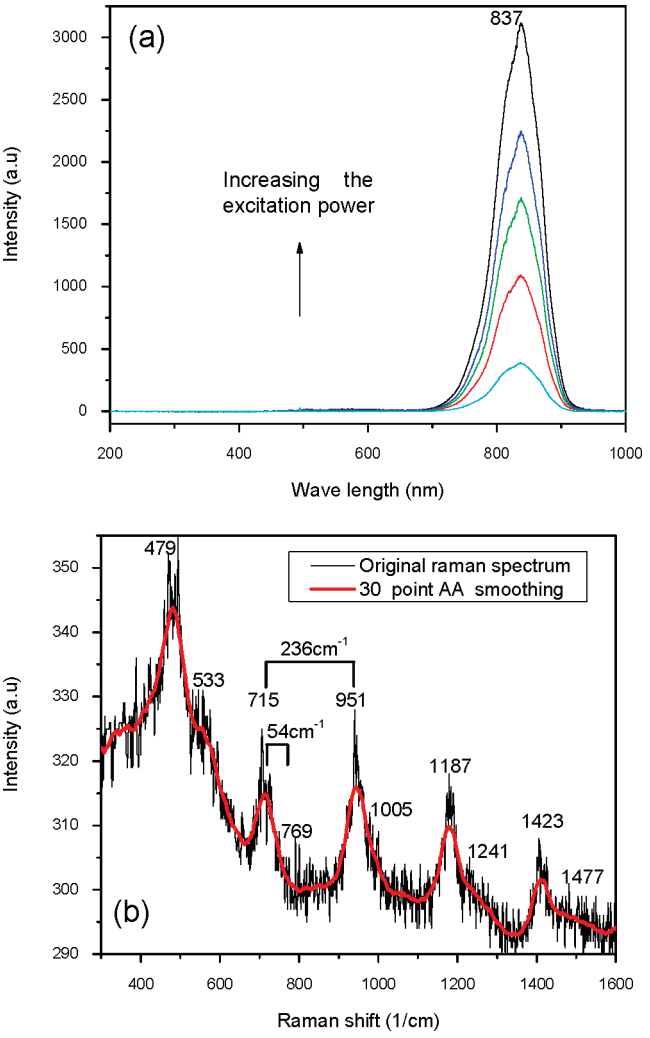

Figure 6. (a) The PL spectra of doped ZnTe microstructures with 1.86% In under different excitation power at room temperature. (b) The corresponding Raman spectrum with 488 nm (Ar^+ laser) as the excitation source.

excitation like excitons. According to our present PL results, we can estimate the indium donor level located less than 0.4 eV beneath the conduction band, which is also consistent with the value of 0.5 eV in In-ZnS phosphors.[31] Furthermore, the fwhm (about 89 nm) in doped microstructures is larger than that of pure ZnTe microstructures, which is also a consequence of a strong exciton coupling with the lattice, as well as the presence of defect complexes with slightly separated energy levels. In addition, different from the band edge emission of pure ZnTe microstructures, these emission peaks of doped ZnTe show no redshift under rising excitation power, which demonstrates their local trapping nature in the microstructures. Due to the In(III) (acceptor center) existence, this transition may not be from a DX state with delocalized nature, but a possible DA pair(DAP) with local transition. The In(I)−In(III) pair may be one possible channel for the band at 713 nm located at the high excitation power. Such red emission in the doped ZnTe microstructures may work as that of CdSe[5] or Se-CdS[17] nanostructures and substitute for the heavy metals in them.

Figure 6a shows the PL spectra of doped microstructures with 1.86% In concentration (sample B). We observe the emission band maximum shift to 837 nm and we observe no shift under

dx.doi.org/10.1021/jp1069237 |J. Phys. Chem. C 2011, 115, 1415–1421

rising excitation power, while we cannot observe the band-edge emission. Compared with the emission of sample A with 1.15% In, this PL shows infrared emission and the emission color cannot be seen by the naked eye, which is consistent with the black color of the sample. Similar to red emission, this infrared emission can be attributed to recombination between indium donor and deep-lying acceptors, such as Y band, which usually appear in wide bandgap semiconductors.[32,33] The Y band is related to the lattice imperfection, structure defects, and dislocation, and locates at about 170−270 meV above the valence band.[34−36] Here the In(III) may be the dominant acceptor. The optical characteristics of the Y band strongly depend on the impurity density and growth conditions. Our doping process not only produced the diffusion of In, but also introduced the high density of defect states, such as: Zn vacancy (V_{zn}) or aggregated In pairs. Therefore, the intensity of trapping states is higher when more In is doped into the ZnTe crystal. Careful observation shows that the infrared emissions at above 800 nm also exist in sample A, which can be divided into more emission bands, see the upper inset in Figure 5. These results reflected multi-DA pairs in this doping sample, like the In(0)−In(III) pair, because the radiative charge transfer transition between D and A determines the location of the emission wavelength. When the In concentration increase, more In(0) and In pairs populate, so the In(0)−In(III) pair may be dominant over the In(I)−In(III) pair, therefore producing the emission at 837 nm. The color of the sample becomes dark black, which also proves this tendency. Moreover, the In(0) has two electrons ready to be released, its emission (Figure 6) should be stronger than that (Figure 5) of In(I) at the start. Therefore, the donor−acceptor (Y band) complex emission under higher dopant concentration reflected an In valence state modulation in the ZnTe doping microstructures, producing a redshift emission.

Multiphonon often occurs in the local exciton excitation case.[37] Figure 6b is the Raman spectrum of sample B, which was obtained by using 488 nm as the excitation source. Several sharp vibration modes in the Raman spectrum are detected, which are at 479, 715, 951, 1187, 1423 cm^{-1} and corresponding shoulder peaks locate at 533, 769, 1005, 1241, 1477 cm^{-1}, respectively. Irwin et. al investigated the Raman scattering of ZnTe systematically and listed many vibration modes of ZnTe crystal, such as LO(Γ)-208 cm^{-1}, TO(Γ)-178 cm^{-1}, LO(X)-182 cm^{-1}, TO(X)-173 cm^{-1}, LA(X)-143 cm^{-1}, TA(X)-54 cm^{-1}, LO(L)-172 cm^{-1}, TO(L)-171 cm^{-1}, LA(L)-154 cm^{-1}, TA(L)-46 cm^{-1}, 228 cm^{-1}-TO(X)+TA(X), 240 cm^{-1}-LO(X)+TA(X).[38] In our present results, the differences between neighboring sharp vibration modes are uniform at 236 cm^{-1}, which is consistent with the TA(X)+TO(X) mode. The difference between sharp vibration modes and their corresponding shoulder peaks is 54 cm^{-1}, which equals TA(X). We also do Raman scattering measurement in sample A, but cannot observe any Raman peaks due to its strong emission. This is because its emission band is close to the Raman scattering peaks. The weak acoustic phonon mode observed in our doped ZnTe microstructures comes from the doping effect and the resulting selection rule relaxation. Local vibration enhancement always accompanies the acoustic modes and multiphonon scattering in doped nanostructures or layer-like structures.[39,40] Therefore, the acoustic mode and the optical mode combine and appear together in the microstructures, verifying that the impurity ion doped into the ZnTe crystal and therein induced multilayered periodical structures. We also see that the phonon overtone

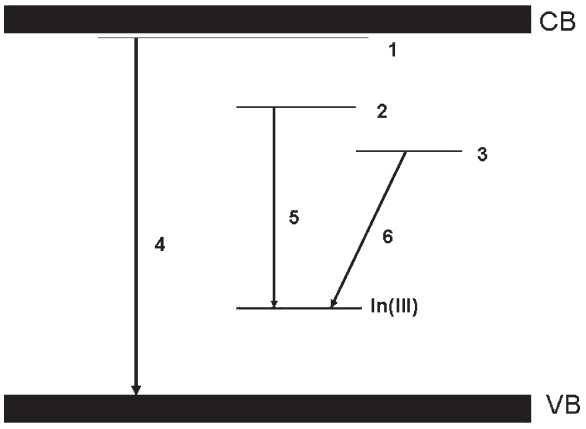

Figure 7. The electronic level diagram of ZnTe:In crystal. (1) Shallow trap level; (2) In(I) state level; (3) In(0) or aggregate level; (4) bandedge radiation transition; and (5 and 6) DAP transition.

intensity has an unstriking monotonic decrease in the Raman spectrum. This can be explained by the phenomenon of outgoing resonance (matching of the excitation energy to electronic transitions), where incoming photon energy E_{in} (488 nm) is scattered m times by phonons giving its final energy E_{out} (837 nm), that is, $E_{out} = E_{in} - mh\omega$. Therefore, the intensity of the phonon line is determined by the product of a term which resonates at $m\omega$ and a term which decays as rapidly as m^{-4}—the competition between resonance and decay with order number. The Raman spectrum with multipeaks also confirms the multiphonon process (that is: $m > 1$). For the local deeptrap transition, the multiphonon process is well-defined in the nonradiative process,[37] in good agreement with our experiments. Therefore, Figure 7 can be drawn with a energy level diagram of ZnTe:In crystal to describe the photon excitation and emission process, different transitions can be illustrated in it. For the In doping and color center formation, the DAP process can be observed with tunable emissions in the microstructure for the first time.

4. CONCLUSIONS

In summary, we have successfully synthesized high-purity and doped ZnTe microstructures, respectively. The morphology of doped ZnTe microstructures shows multilayered periodical structure, which is due to the dopant ion resulting in lattice mismatch and is different from the morphology of pure ZnTe microstructures. The PL spectra of pure ZnTe microstructures show band-edge or near band-edge emission under different excitation powers while the PL spectra of doped ZnTe microstructures with different dopant concentrations show red or infrared emission. The red or infrared emissions are related to the recombination between In donor levels and acceptor levels at varied doping concentrations, respectively. The appearance of acoustic phonon modes and multiphonon scattering in the Raman spectrum of doped ZnTe microstructures confirm that In doping into the ZnTe lattice occurs effectively and with clear local carrier trapping. The present results indicate that the DAP state incorporated in microstructures with tunable emissions may find application in future display device design.

AUTHOR INFORMATION

Corresponding Author

*E-mail: zoubs@bit.edu.cn.

■ ACKNOWLEDGMENT

We thank the NSF of China (Term Nos. 90606001, 20873039, 90406024, 90923014, and 10974050), Hunan Provincial Natural Science Foundation (07JJ4002 and 09JJ1009), New Century Excellent Talents in University (NCET-08-0182), and Science and Technology Innovative Research Team in Higher Educational Instituions of Hunan Province for financial support.

■ REFERENCES

(1) Wang, Z. L.; *Nanowires and Nanobelts, Vol. II: Nanowires and Nanobelts of Functional Materials*; Kluwer Academic: New York, 2006.
(2) Xia, Y. N.; Yang, P. D.; Sun, Y. G.; Wu, Y. Y.; Mayers, B.; Gates, B.; Yin, Y. D.; Kim, F.; Yan, H. Q. *Adv. Mater.* **2003,** *15*, 353.
(3) Li, Y.; Qian, F.; Xiang, J.; Lieber, C. M. *Mater. Today* **2006,** *9*, 18.
(4) Thelander, C.; Agarwal, P.; Brongersma, S.; Eymery, J.; L. Feiner, F.; Forchel, A.; Scheffler, M.; Riess, W.; Ohlsson, B. J.; Gösele, U.; Samuelson, L. *Mater. Today* **2006,** *9*, 28.
(5) Pan, A. L.; Liu, R. B.; Zhang, Q. L.; Wan, Q.; He, P. B.; Zacharias, M.; Zou, B. S. *J. Phys. Chem. C* **2007,** *111*, 14253.
(6) Pan, A. L.; Liu, D.; Liu, R. B.; Wang, F. F.; Zhu, X.; Zou, B. S. *Small* **2005,** *1*, 980.
(7) Singh, A.; Li, X. Y.; Protasenko, V.; Galantai, G.; Kuno, M.; Xing, H. L.; Jena, D. *Nano Lett.* **2007,** *7*, 2999.
(8) Wang, Y. G.; Zou, B. S.; Wang, T. H.; Wang, N.; Cai, Y.; Chan, Y. F.; Zhou, S. X. *Nanotechnology* **2006,** *17*, 2420.
(9) Tanaka, T.; Matsuno, Y. J.; Kume, Y.; Nishio, M.; Guo, Q. X.; Ogawa, H. *Phys. Status Solidi B* **2004,** *1*, 1026.
(10) Bozzini, B.; Baker, M. A.; Cavallotti, P. L.; Cerri, E.; Lenardi, C. *Thin Solid Films* **2000,** *388*, 361.
(11) Sato, K.; Adachi, S. *J. Appl. Phys.* **1993,** *73*, 926.
(12) Chang, J. H.; Cho, M. W.; Wang, H. M.; Wenisch, H.; Hanada, T.; Yao, T.; Sato, K.; Oda, O. *Appl. Phys. Lett.* **2000,** *77*, 1256.
(13) Li, L.; Yang, Y. W.; Huang, X. H.; Li, G. H.; Zhang, L. D. *J. Phys. Chem. B* **2005,** *109*, 12394.
(14) Yong, K. T.; Sahoo, Y.; Zeng, H.; Swihart, M. T.; Minter, J. R.; Prasad, P. N. *Chem. Mater.* **2007,** *19*, 4108.
(15) Zhang, J.; Sun, K.; Kumbhar, A.; Fang, J. Y. *J. Phys. Chem. C* **2008,** *112*, 5454.
(16) Huo, H. B.; Dai, L.; Xia, D. Y.; Ran, G. Z.; You, L. P.; Zhang, B. R.; Qin, G. G. *J. Nanosci. Nanotechnol.* **2006,** *6*, 1182.
(17) Pan, A. L.; Wang, X.; He, P. B.; Zhang, Q. L.; Wan, Q.; Zacharias, M.; Zhu, X.; Zou, B. S. *Nano Lett.* **2007,** *7*, 2970.
(18) Pradhan, N.; Peng, X. G. *J. Am. Chem. Soc.* **2007,** *129*, 3339.
(19) Tokumoto, M. S.; Smith, A.; Santilli, C. V.; Pulcienlli, S. H.; Elkaim, E.; Briois, V. *J. Non-Cryst. Solids* **2000,** *273*, 302.
(20) Yan, Y. G.; Zhang, Y.; Zeng, H. B.; Zhang, L. D. *Cryst. Growth Des.* **2007,** *7*, 940.
(21) Xu, D.; Shi, X.; Guo, G.; Gui, L.; Tang, Y. *J. Phys. Chem. B* **2000,** *104*, 5061.
(22) Lu, F; Cai, W. P.; Zhang, Y. G.; Li, Y; Sun, F. Q.; Heo, S. H.; Cho, S. O. *Appl. Phys. Lett.* **2006,** *89*, 231928.
(23) Yoshino, K.; Yoneta, M.; Arakawa, A.; Ohmori, K.; Saito, H.; Ohisihi, M. *Phys. Status Solidi* **2003,** *(c)0(2)*, 631.
(24) http://www.springermaterials.com/pdfs/10.1007/978-3-540-74392-7_211.pdf
(25) Puthussery, J.; Lan, A.; Kosel, T. H.; Kuno, M. *ACS Nano* **2008,** *2* (2), 357–367.
(26) Haug, H.; Koch, S. W.; *Quantum Theory of the Optical and Electronic Properties of Semiconductors*, 4th ed.; World Scientific: Singapore, 2004.
(27) Cheng, B.; Han, Z.; Guo, H.; Lin, S.; Zhang, Z.; Xiao, Y.; Lei, S. *J. Appl. Phys.* **2010,** *108*, 014309.
(28) Garcia, J. A.; Remon, A.; Munoz, V; Triboulet, R. *J. Cryst. Growth* **1998,** *191*, 685–691.
(29) Nicholls, J. E.; Davies, J. J. *J. Phys. C: Solid State Phys.* **1980,** *13*, 2393.
(30) Karczewski, G.; Zakrzewski, A. K.; Dobaczewski, L.; Dobrowolski, W.; Jaroszyfiski, J.; Wojtowicz, T.; Kossut, J. *Thin Solid Films* **1995,** *267*, 79.
(31) Apple, E. F.; Williams, F. E. *J. Electrochem. Soc.* **1959,** *106*, 224.
(32) Trager, C. C.; Burley, A.; Donnell, K. P. O.; Naumov, A.; Wolf, K.; Stanzl, H. P.; Wagner, H. P.; Gebhardt, W. *Microsc. Semicond. Mater.* **1993,** *134*, 683.
(33) Fernández, P.; Garcia, J. A.; Remón, A.; Piqueras, J.; Muñoz, V.; Triboulet, R. *Semicond. Sci. Technol.* **1998,** *13*, 410.
(34) Luo, M.; Vanmil, B. L.; Tompkins, R. P.; Myers, T. H.; Giles, N. C. *J. Appl. Phys.* **2005,** *97*, 013518.
(35) Yu, Y. M.; Nam, S. G.; Lee, K. S.; Choi, Y. D.; Byungsung, O. *J. Appl. Phys.* **2001,** *90*, 807.
(36) Kvit, A. V.; Medvedev, S. A.; Klevkov, Y. V.; Zatsev, V. V.; Onishchenko, E. E.; Klokov, A. V.; Bagaev, V. S.; Tsikunov, A. V.; Perestoronin, A. V.; Yakimov, M. V. *Phys. Solid State* **1998,** *40*, 924.
(37) Pässler, R. *Phys. Status Solidi B* **1976,** *78*, 625–63510.1002/pssb.2220780222.
(38) Irwin, J. C.; Lacombe, J. *J. Appl. Phys.* **1970,** *41*, 1444.
(39) Walukiewicz, W. *Phys. Rev. B* **1988,** *37*, 8530.
(40) Glavin, B. A.; Kochelap, V. A.; Linnik, T. L.; Kim, K. W.; Stoscio, M. A. *Phys. Rev. B* **2002,** *65*, 085303.